JOURNAL OF GUIDANCE, CONTROL, AND DYNAMICS
Vol. 26, No. 2, March–April 2003

Output Feedback Control of Mechanical Systems with Application to Spacecraft and Robots

F. Caccavale*
Università degli Studi della Basilicata, 85100 Potenza, Italy
C. Natale†
Seconda Università degli Studi di Napoli, 81031 Aversa, Italy
and
L. Villani‡
Università degli Studi di Napoli Federico II, 80125 Napoli, Italy

The motion control problem for a class of mechanical systems is addressed. The system configuration can be represented in terms of a set of generalized coordinates in $\mathbb{R}^n$ and l rotation matrices in the special orthogonal (SO)(3) group. A key point is the choice of a globally valid parameterization of SO(3) in lieu of the usual three-parameter representations. To this end, the unit quaternion is adopted. A novel control law is proposed that is based on a velocity observer to avoid velocity measurements. Exponential tracking of the commanded motion trajectory is proven via the Lyapunov direct method. The proposed controller–observer scheme is first applied in a simulation case study to the attitude control of a rigid spacecraft. Then, the problem of position and orientation control of the end effector of a robot manipulator is considered. For the latter case, experimental results are provided to show the potential of the approach in tackling practical problems.

I. Introduction

MOTION control of articulated mechanical systems is a crucial issue for a wide range of applications, for example, robotics and autonomous vehicle–manipulator systems for underwater and space applications.

The common feature of this class of mechanical systems is that they consist of a number of rigid bodies coupled to each other. The system configuration can be related to a set of n generalized coordinates belonging to $\mathbb{R}^n$, together with l rotation matrices belonging to the special orthogonal (SO)(3) group. These matrices describe the attitude of l bodies of interest in the system. Therefore, the configuration space can be represented by the Cartesian product $\mathbb{R}^n \times \mathrm{SO}(3)^l$ (see Ref. 1).

A simple example is given by a free-floating rigid body, for example, a rigid spacecraft, whose configuration can be represented in terms of a rotation matrix describing the orientation of a body-fixed frame with respect to a reference frame ($l = 1$). Another example is represented by a six-degree-of-freedom robot manipulator, which can be modeled in terms of end-effector position ($n = 3$) and orientation ($l = 1$). Also, the configuration space of a six-degree-of-freedom manipulator mounted on a floating base, for example, an underwater vehicle–manipulator system, is given by $\mathbb{R}^6 \times \mathrm{SO}(3)^2$; in this case the position of the manipulator's tip and of the base ($n = 6$) are of interest, as well as the end-effector orientation and the base attitude ($l = 2$).

For the preceding class of mechanical systems, the motion control objective consists of tracking the desired trajectories for the n generalized coordinates and the desired attitude trajectories for the l rigid bodies. For control design purposes, a major problem is the choice of a singularity-free parameterization of SO(3). A minimal parameterization in terms of three variables for example, Euler angles, leads to a mapping between SO(3) and $\mathbb{R}^3$, which is singular for some configurations (representation singularities). Therefore, it is convenient to adopt a nonminimal parameterization that provides a global representation of the SO group of rotations. To this end, the unit quaternion[2] has been widely adopted to develop control algorithms both in SO(3) (Refs. 3–5) and in $\mathbb{R}^n \times \mathrm{SO}(3)^l$ (Ref. 1).

Tracking control strategies typically require full-state measurements, that is, the n generalized coordinates, the orientation of the l frames, and the corresponding velocities. However, velocity measurements are often not available and they are usually replaced by numerical derivatives of the measured configuration coordinates. This may lead to chattering of the control inputs due to the combined effect of measurements noise and quantization. Indeed, high-frequency chattering is usually filtered out by the system but may cause high power consumption and actuator wear and may magnify the effects of other phenomena, for example, friction and elasticity.

To avoid this undesirable behavior, the use of suitable velocity estimates via nonlinear observers or lead filters in the feedback loop have been proposed for the attitude control problem.[6–8] In the framework of robot manipulator motion control, both joint space[9–11] and task space[12] approaches have been pursued; also, adaptive[13] and neural network[14] output feedback schemes have been devised.

In this paper, the problem of tracking control of mechanical systems in the absence of velocity measurements is addressed. The proposed approach extends the results presented in Ref. 15 for the case of attitude control of a spacecraft to the general case of motion control of articulated mechanical systems in $\mathbb{R}^n \times \mathrm{SO}(3)^l$. In Ref. 15, two alternative output feedback schemes were proposed: The first was based on the passivity properties of rigid-body dynamics and the second was based on a proportional derivative control law with nonlinear feedforward compensation. The performance of the two schemes was tested in simulation and similar results were obtained. To exploit the passivity properties of mechanical systems fully (see Ref. 16 and the references therein), the first output feedback scheme is further investigated and extended to a more general class of mechanical systems. A passivity-based control law is designed in detail, together with a nonlinear observer; then, the two algorithms are tuned to each other to achieve exponential convergence of both tracking and estimation errors. The stability analysis is carried out by using the Lyapunov direct method, and sufficient conditions ensuring exponential stability are derived.

Received 30 September 2001; revision received 30 May 2002; accepted for publication 3 October 2002. Copyright © 2002 by the American Institute of Aeronautics and Astronautics, Inc. All rights reserved. Copies of this paper may be made for personal or internal use, on condition that the copier pay the $10.00 per-copy fee to the Copyright Clearance Center, Inc., 222 Rosewood Drive, Danvers, MA 01923; include the code 0731-5090/03 $10.00 in correspondence with the CCC.

*Professor, Dipartimento di Ingegneria e Fisica dell'Ambiente, Contrada Macchia Romana; caccaval@unina.it.
†Assistant Professor, Dipartimento di Ingegneria dell'Informazione, Via Roma 29; cinatale@unina.it.
‡Professor, Dipartimento di Informatica e Sistemistica, Via Claudio 21; lvillani@unina.it.

To better understand the benefits of the proposed approach, the controller–observer algorithm is tested in a number of case studies and compared to a passivity-based controller requiring full-state feedback, where the estimate of velocity is achieved from position measurements using a simple linear filter. Both simulations and experimental results show a significant improvement of performance of the output feedback control and confirm that the absence of velocity measurements has to be considered carefully for control design purposes.

The paper is organized as follows. In Sec. II, the dynamic model of an articulated mechanical system is developed in terms of a suitable set of generalized coordinates. In Sec. III, the design of the passivity-based controller–observer algorithm is presented. In Sec. IV, the analysis of two case studies is carried out: First, the attitude control problem of a rigid spacecraft in the presence of measurements noise and quantization effects is considered and simulation results are presented; then, the position and orientation control problem of the end effector of a six-degree-of-freedom robot manipulator is tackled and both simulation and experimental results are presented. Finally, some useful properties of the unit quaternion are summarized in Appendix A, and Appendix B reports the stability proof.

II. Modeling

Consider an articulated mechanical system composed of a number of rigid bodies coupled to each other. Let $\boldsymbol{x} \in \mathbb{R}^n$ denote a vector of generalized coordinates for the system (e.g., position of some rigid bodies in the system, position/rotation of mechanical joints) and define the $(3l \times 3l)$ matrix

$$\boldsymbol{R}^0 = \operatorname{diag}\left\{\boldsymbol{R}_1^0, \ldots, \boldsymbol{R}_l^0\right\} \tag{1}$$

where $\boldsymbol{R}_i^0 \in \mathrm{SO}(3)$ are the rotation matrices representing the orientation of l coordinate frames $\Sigma_1, \ldots, \Sigma_l$, each attached to the corresponding rigid body with respect to a common reference frame Σ_0. Hereafter, the superscript 0 will denote that the corresponding quantities are expressed in the frame Σ_0; the superscript will be dropped whenever a quantity is referred to a frame Σ_i.

The $(p \times 1)$ velocity vector of the system, with $p = n + 3l$, is defined as

$$\boldsymbol{v} = \begin{bmatrix} \dot{\boldsymbol{x}} \\ \boldsymbol{\omega} \end{bmatrix} \tag{2}$$

where

$$\boldsymbol{\omega} = \begin{bmatrix} \boldsymbol{\omega}_1 \\ \vdots \\ \boldsymbol{\omega}_l \end{bmatrix} \tag{3}$$

is the stacked vector collecting the l angular velocities of the rigid bodies, expressed in the corresponding body-fixed frames, that is, $\boldsymbol{\omega}_i = \boldsymbol{R}_i^{0T} \boldsymbol{\omega}_i^0$. The angular velocities satisfy the equation

$$\dot{\boldsymbol{R}}_i^0 = \boldsymbol{R}_i^0 \boldsymbol{S}_3(\boldsymbol{\omega}_i), \qquad i = 1, \ldots, l \tag{4}$$

where $\boldsymbol{S}_3(\cdot)$ is the (3×3) skew-symmetric matrix operator performing the cross product.

The equations of motion for the class of mechanical systems considered here can be expressed in the form[1]

$$\boldsymbol{M}(\mathcal{X})\dot{\boldsymbol{v}} + \boldsymbol{C}(\mathcal{X}, \boldsymbol{v})\boldsymbol{v} + \boldsymbol{g}(\mathcal{X}) = \boldsymbol{u} \tag{5}$$

where the set $\mathcal{X} = \{\boldsymbol{x}, \boldsymbol{R}^0\}$ describes the system configuration, $\boldsymbol{M}(\mathcal{X}) \in \mathbb{R}^{p \times p}$ is the inertia matrix, $\boldsymbol{C}(\mathcal{X}, \boldsymbol{v}) \in \mathbb{R}^{p \times p}$ is the matrix of centrifugal and Coriolis terms, $\boldsymbol{g}(\mathcal{X}) \in \mathbb{R}^p$ is the vector of the potential forces, and $\boldsymbol{u} \in \mathbb{R}^p$ is the vector of input generalized forces provided by the actuators.

It is assumed that the following properties hold:

Property 1: The matrix $\boldsymbol{M}$ is symmetric and positive definite; moreover, it satisfies the inequality $M_m \le \|\boldsymbol{M}\| \le M_M$, where M_m (M_M) is the minimum (maximum) eigenvalue of $\boldsymbol{M}$.

Property 2: For a suitable parameterization of $\boldsymbol{C}$, the matrix $\dot{\boldsymbol{M}} - 2\boldsymbol{C}$ is skew symmetric, which implies that $\dot{\boldsymbol{M}} = \boldsymbol{C} + \boldsymbol{C}^T$.

Property 3: The matrix $\boldsymbol{C}$ satisfies the inequality

$$\|\boldsymbol{C}(\mathcal{A}, \boldsymbol{b})\boldsymbol{c}\| \le C_M \|\boldsymbol{b}\| \|\boldsymbol{c}\|$$

and the equality

$$\boldsymbol{C}(\mathcal{A}, \alpha_1 \boldsymbol{b} + \alpha_2 \boldsymbol{c}) = \alpha_1 \boldsymbol{C}(\mathcal{A}, \boldsymbol{b}) + \alpha_2 \boldsymbol{C}(\mathcal{A}, \boldsymbol{c})$$

Note that for systems containing kinematic chains, for example, robot manipulators, the dynamic model (5) and the related properties may become not well-defined at configurations corresponding to kinematic singularities.[17] This problem is very challenging and can be addressed by adopting different approaches (see Ref. 18 and references therein). Namely, if motion planning is performed offline, the occurrence of kinematic singularities can be avoided via a careful choice of the desired trajectory. In the case of real-time motion planning, effective and reliable solutions have been proposed, for example, for the case of resolved acceleration control.[19]

Throughout the paper, a quaternion-based description of the rigid-body attitude is used.[2] In fact, the use of the unit quaternion in lieu of a minimal representation of the orientation (for example, Euler angles) allows overcoming problems arising from representation singularities; also, the unit quaternion possesses useful properties[20] that allow reduction of the computational burden and lead to a more compact formulation of the control law. A few basic concepts regarding unit quaternions are summarized in Appendix A.

III. Control

The control objective consists of tracking a desired trajectory $\boldsymbol{x}_d(t)$ for the generalized coordinates and l desired attitude trajectories, specified in terms of the unit quaternions $\mathcal{Q}_{di}(t)$, $i = 1, \ldots, l$, without using velocity feedback. The desired velocity vector for the generalized coordinates is $\dot{\boldsymbol{x}}_d(t)$, whereas the vector $\boldsymbol{\omega}_d^0(t) = [\boldsymbol{\omega}_{d1}^{0T}(t), \ldots, \boldsymbol{\omega}_{dl}^{0T}(t)]^T$ represents the desired angular velocities. The desired accelerations are assigned in terms of the vectors $\ddot{\boldsymbol{x}}_d(t)$ and $\dot{\boldsymbol{\omega}}_d^0(t)$.

The desired angular velocities are naturally assigned with respect to the frame Σ_0. To preserve consistency with the dynamic model (5), the angular velocities are to be referred to the body-fixed frames $\Sigma_1, \ldots, \Sigma_l$, that is,

$$\boldsymbol{\omega}_d = \boldsymbol{R}^{0T} \boldsymbol{\omega}_d^0 \tag{6}$$

Therefore, the desired velocity vector is defined as

$$\boldsymbol{v}_d = \begin{bmatrix} \dot{\boldsymbol{x}}_d \\ \boldsymbol{\omega}_d \end{bmatrix} \tag{7}$$

It assumed that $\|\boldsymbol{v}_d(t)\| \le v_{dM}$ for all $t \ge 0$.

The computation of the time derivative $\dot{\boldsymbol{\omega}}_d$ in body-fixed coordinates requires knowledge of the actual angular velocities. To overcome this problem, a suitable feedforward acceleration vector has to be used in lieu of $\dot{\boldsymbol{\omega}}_d$, namely,

$$\boldsymbol{a}_d = \begin{bmatrix} \ddot{\boldsymbol{x}}_d \\ \boldsymbol{R}^{0T} \dot{\boldsymbol{\omega}}_d^0 - \boldsymbol{S}(\boldsymbol{\omega}_d) \boldsymbol{R}^{0T} \boldsymbol{\omega}_d^0 \end{bmatrix} \tag{8}$$

which can be evaluated without using the actual angular velocities. In Eq. (8), it is $\boldsymbol{S}(\boldsymbol{\omega}_d) = \operatorname{diag}\{\boldsymbol{S}_3(\boldsymbol{\omega}_{d1}), \ldots, \boldsymbol{S}_3(\boldsymbol{\omega}_{dl})\}$.

Note that $\dot{\boldsymbol{v}}_d$ and $\boldsymbol{a}_d$ are related by the equality

$$\dot{\boldsymbol{v}}_d = \boldsymbol{a}_d + \boldsymbol{S}_O(\tilde{\boldsymbol{\omega}}_d)\boldsymbol{v}_d \tag{9}$$

where $\boldsymbol{S}_O(\cdot) = \operatorname{diag}\{\boldsymbol{O}_n, \boldsymbol{S}(\cdot)\}$, $\boldsymbol{O}_n$ is the $(n \times n)$ null matrix, and $\tilde{\boldsymbol{\omega}}_d = \boldsymbol{\omega}_d - \boldsymbol{\omega}$.

A. Control Law

In the absence of velocity measurements, it is necessary to resort to an observer that provides a velocity estimate

$$\boldsymbol{v}_e = \begin{bmatrix} \dot{\boldsymbol{x}}_e \\ \boldsymbol{\omega}_e \end{bmatrix} \tag{10}$$

Let $\boldsymbol{x}_e$ denote the estimated generalized coordinates and $\mathcal{Q}_{ei}$, $i = 1, \ldots, l$, the estimated attitude of the ith rigid body. The tracking and estimation error vectors are defined as

$$\boldsymbol{e}_d = \begin{bmatrix} \tilde{\boldsymbol{x}}_d \\ \tilde{\boldsymbol{\epsilon}}_d \end{bmatrix}, \qquad \boldsymbol{e}_e = \begin{bmatrix} \tilde{\boldsymbol{x}}_e \\ \tilde{\boldsymbol{\epsilon}}_e \end{bmatrix} \tag{11}$$

where

$$\tilde{\boldsymbol{x}}_d = \boldsymbol{x}_d - \boldsymbol{x} \tag{12}$$

$$\tilde{\boldsymbol{x}}_e = \boldsymbol{x}_e - \boldsymbol{x} \tag{13}$$

and $\tilde{\boldsymbol{\epsilon}}_d$ and $\tilde{\boldsymbol{\epsilon}}_e$ are obtained by stacking the vector parts of the unit quaternions, $i = 1, \ldots, l$,

$$\tilde{\mathcal{Q}}_{di} = \mathcal{Q}_i^{-1} \times \mathcal{Q}_{di} \tag{14}$$

$$\tilde{\mathcal{Q}}_{ei} = \mathcal{Q}_i^{-1} \times \mathcal{Q}_{ei} \tag{15}$$

whereas $\tilde{\boldsymbol{\eta}}_d$ and $\tilde{\boldsymbol{\eta}}_e$ are obtained by stacking their scalar parts. Also, consider the corresponding vectors of velocity errors

$$\tilde{\boldsymbol{v}}_d = \begin{bmatrix} \dot{\tilde{\boldsymbol{x}}}_d \\ \tilde{\boldsymbol{\omega}}_d \end{bmatrix} = \boldsymbol{v}_d - \boldsymbol{v} \tag{16}$$

$$\tilde{\boldsymbol{v}}_e = \begin{bmatrix} \dot{\tilde{\boldsymbol{x}}}_e \\ \tilde{\boldsymbol{\omega}}_e \end{bmatrix} = \boldsymbol{v}_e - \boldsymbol{v} \tag{17}$$

To avoid direct velocity feedback, the following error vector is used in the control law

$$\boldsymbol{e}_{de} = \begin{bmatrix} \tilde{\boldsymbol{x}}_{de} \\ \tilde{\boldsymbol{\epsilon}}_{de} \end{bmatrix} \tag{18}$$

where $\tilde{\boldsymbol{x}}_{de} = \boldsymbol{x}_d - \boldsymbol{x}_e = \tilde{\boldsymbol{x}}_d - \tilde{\boldsymbol{x}}_e$, and $\tilde{\boldsymbol{\epsilon}}_{de}$ is obtained by stacking the vector parts of the unit quaternions, $i = 1, \ldots, l$,

$$\mathcal{Q}_{ei}^{-1} \times \mathcal{Q}_{di} = \tilde{\mathcal{Q}}_{ei}^{-1} \times \tilde{\mathcal{Q}}_{di} \tag{19}$$

Moreover, the following velocity vectors are introduced:

$$\boldsymbol{v}_r = \boldsymbol{v}_d + \boldsymbol{\Lambda}_d \boldsymbol{e}_{de} \tag{20}$$

$$\boldsymbol{v}_o = \boldsymbol{v}_e + \boldsymbol{\Lambda}_e \boldsymbol{e}_e \tag{21}$$

which can be evaluated without using the actual velocity $\boldsymbol{v}$. In Eqs. (20) and (21) the matrices

$$\boldsymbol{\Lambda}_d = \text{diag}\{\boldsymbol{\Lambda}_{dX}, \lambda_{dO1}\boldsymbol{I}_3, \ldots, \lambda_{dOl}\boldsymbol{I}_3\}$$

$$\boldsymbol{\Lambda}_e = \text{diag}\{\boldsymbol{\Lambda}_{eX}, \lambda_{eO1}\boldsymbol{I}_3, \ldots, \lambda_{eOl}\boldsymbol{I}_3\}$$

are diagonal and positive definite.

The proposed control law, which can be framed in the passivity approach,[16] is

$$\boldsymbol{u} = \boldsymbol{M}(\mathcal{X})\boldsymbol{a}_r + \boldsymbol{C}(\mathcal{X}, \boldsymbol{v}_o)\boldsymbol{v}_r + \boldsymbol{K}_v(\boldsymbol{v}_r - \boldsymbol{v}_o) + \boldsymbol{K}_p\boldsymbol{e}_d + \boldsymbol{g}(\mathcal{X}) \tag{22}$$

where $\boldsymbol{K}_p = \text{diag}\{\boldsymbol{K}_{pX}, k_{pO1}\boldsymbol{I}_3, \ldots, k_{pOl}\boldsymbol{I}_3\}$, and $\boldsymbol{K}_v$ are symmetric positive-definite matrices, and

$$\boldsymbol{a}_r = \boldsymbol{a}_d + \boldsymbol{\Lambda}_d \dot{\boldsymbol{e}}_{de} \tag{23}$$

Notice that the control law (22) requires direct feedback of sole vehicle position and orientation.

The estimated velocity $\boldsymbol{v}_e$ is obtained via the observer defined by the equations

$$\dot{\boldsymbol{z}} = \boldsymbol{M}(\mathcal{X})\boldsymbol{a}_r - (\boldsymbol{L}_p + \boldsymbol{L}_v\boldsymbol{A}(\tilde{\boldsymbol{\eta}}_e, \tilde{\boldsymbol{\epsilon}}_e)\boldsymbol{\Lambda}_e)\boldsymbol{e}_e + \boldsymbol{K}_p\boldsymbol{e}_d + \boldsymbol{C}(\mathcal{X}, \boldsymbol{v}_o)\boldsymbol{v}_r + \boldsymbol{C}^T(\mathcal{X}, \boldsymbol{v}_r)\boldsymbol{v}_o$$

$$\boldsymbol{v}_e = \boldsymbol{M}^{-1}(\mathcal{X})(\boldsymbol{z} - \boldsymbol{L}_v\boldsymbol{e}_e) - \boldsymbol{\Lambda}_e\boldsymbol{e}_e \tag{24}$$

In Eqs. (24), the matrices

$$\boldsymbol{L}_p = \text{diag}\{\boldsymbol{L}_{pX}, l_{pO1}\boldsymbol{I}_3, \ldots, l_{pOl}\boldsymbol{I}_3\}$$

$$\boldsymbol{L}_v = \text{diag}\{\boldsymbol{L}_{vX}, l_{vO1}\boldsymbol{I}_3, \ldots, l_{vOl}\boldsymbol{I}_3\}$$

are symmetric and positive definite, and

$$\boldsymbol{A}(\tilde{\boldsymbol{\eta}}_e, \tilde{\boldsymbol{\epsilon}}_e) = \begin{bmatrix} \boldsymbol{I}_n & \boldsymbol{O} \\ \boldsymbol{O}^T & \boldsymbol{E}(\tilde{\boldsymbol{\eta}}_e, \tilde{\boldsymbol{\epsilon}}_e)/2 \end{bmatrix} \tag{25}$$

where $\boldsymbol{O}$ denotes a null matrix of proper dimensions, and the matrix $\boldsymbol{E}$ is defined in Appendix A. The estimated generalized coordinates $\boldsymbol{x}_e$ are computed by integrating the corresponding estimated velocities $\dot{\boldsymbol{x}}_e$, whereas the estimated orientation $\mathcal{Q}_e = \{\mathcal{Q}_{e1}, \ldots, \mathcal{Q}_{el}\}$ is computed from the estimated angular velocities $\boldsymbol{\omega}_e$ by integrating the quaternion propagation rule

$$\dot{\boldsymbol{\eta}}_e = -\tfrac{1}{2}\boldsymbol{N}(\boldsymbol{\epsilon}_e)\boldsymbol{\omega}_e \tag{26}$$

$$\dot{\boldsymbol{\epsilon}}_e = \tfrac{1}{2}\boldsymbol{E}(\boldsymbol{\eta}_e, \boldsymbol{\epsilon}_e)\boldsymbol{\omega}_e \tag{27}$$

where the matrix $\boldsymbol{N}$ is defined in Appendix A.

B. Stability Analysis

In general, the stability of the closed-loop system is not guaranteed for any choice of the controller and observer parameters. Hence, it is worth looking for a region in the parameters space where asymptotic stability is ensured. This goal can be achieved by means of a Lyapunov argument.

To simplify the notation, it is useful to define the variables

$$\boldsymbol{\sigma}_d = \boldsymbol{v}_r - \boldsymbol{v} = \tilde{\boldsymbol{v}}_d + \boldsymbol{\Lambda}_d\boldsymbol{e}_{de} \tag{28}$$

$$\boldsymbol{\sigma}_e = \boldsymbol{v}_o - \boldsymbol{v} = \tilde{\boldsymbol{v}}_e + \boldsymbol{\Lambda}_e\boldsymbol{e}_e \tag{29}$$

When Eq. (8) is folded in Eq. (23), the following equality can be found:

$$\boldsymbol{a}_r = \dot{\boldsymbol{v}}_r + \boldsymbol{S}_O(\tilde{\boldsymbol{\omega}}_d)\boldsymbol{v}_d \tag{30}$$

When Eq. (5) is combined with the control law (22) and equality (30) and property 3 are used, the tracking error dynamics can be derived:

$$\boldsymbol{M}(\mathcal{X})\dot{\boldsymbol{\sigma}}_d + \boldsymbol{C}(\mathcal{X}, \boldsymbol{v})\boldsymbol{\sigma}_d + \boldsymbol{K}_v\boldsymbol{\sigma}_d + \boldsymbol{K}_p\boldsymbol{e}_d = \boldsymbol{K}_v\boldsymbol{\sigma}_e - \boldsymbol{C}(\mathcal{X}, \boldsymbol{\sigma}_e)\boldsymbol{v}_r - \boldsymbol{M}(\mathcal{X})\boldsymbol{S}_O(\tilde{\boldsymbol{\omega}}_d)\boldsymbol{v}_d \tag{31}$$

The observer equation (24), together with Eq. (31) and property 3, provide the estimation error dynamics

$$\boldsymbol{M}(\mathcal{X})\dot{\boldsymbol{\sigma}}_e + (\boldsymbol{L}_v\boldsymbol{A}(\tilde{\boldsymbol{\eta}}_e, \tilde{\boldsymbol{\epsilon}}_e) - \boldsymbol{K}_v)\boldsymbol{\sigma}_e + \boldsymbol{L}_p\boldsymbol{e}_e = -\boldsymbol{K}_v\boldsymbol{\sigma}_d - \boldsymbol{C}(\mathcal{X}, \boldsymbol{v})\boldsymbol{\sigma}_e + \boldsymbol{C}^T(\mathcal{X}, \boldsymbol{\sigma}_d)\boldsymbol{v}_o \tag{32}$$

Hence, a state vector for the closed-loop system (31) and (32) is

$$\boldsymbol{\zeta} = \begin{bmatrix} \boldsymbol{\sigma}_d \\ \boldsymbol{e}_d \\ \boldsymbol{\sigma}_e \\ \boldsymbol{e}_e \end{bmatrix} \tag{33}$$

The following theorem holds.

Theorem 1: There exists a choice of the controller gains $\boldsymbol{K}_p$, $\boldsymbol{K}_v$, and $\boldsymbol{\Lambda}_d$ and of the observer parameters $\boldsymbol{L}_p$, $\boldsymbol{L}_v$, and $\boldsymbol{\Lambda}_e$ such that the origin of the state space of system (31) and (32) is locally exponentially stable.

The proof is given in Appendix B. A simpler stability analysis valid for the particular case of a single rigid body is reported in Ref. 15.

IV. Case Studies

The proposed approach is validated in a number of case studies developed for two typical systems belonging to the class of mechanical systems considered in this paper: a rigid spacecraft and a six-degree-of-freedom robot manipulator.

In the case of the rigid spacecraft, attitude control is of concern ($n = 0$ and $l = 1$). It is assumed that orientation measurements are available and the proposed controller–observer scheme is adopted to overcome the absence of angular velocity measurements. A simulation case study is carried out, taking into account the presence of noise and quantization on the orientation measurements.

For the case of the robot manipulator, the problem of controlling the position and orientation of the end effector is considered ($n = 3$ and $l = 1$). Both a simulation and an experimental study are carried out on an industrial robot Comau SMART-3 S. As for any industrial robot, only joint position measurements are available; hence, the observer–controller algorithm is adopted to achieve end-effector position and attitude trajectory tracking without joint velocity measurements.

The case studies are aimed at showing that the absence of velocity measurements, in the framework of the passivity-based control, cannot be underestimated. To this purpose, the proposed output feedback controller is compared to a passivity-based control strategy requiring full-state feedback, where the absence of velocity measurements is overcome by computing the velocity via a linear first-order filter.

The comparison of the passivity-based control approach with other advanced (full-state or output feedback) control schemes is out of the scope of this paper. The interested reader can find a comparison between the output feedback control algorithm considered in this paper and a different advanced output feedback control scheme in Ref. 15.

A. Rigid Spacecraft

A rigid spacecraft, for example, an unmanned free-flying satellite, can be modeled as a free-floating rigid body whose configuration can be represented in terms of the rotation matrix $\boldsymbol{R}_1^0$, describing the orientation of a frame Σ_1, attached to the spacecraft with respect to a reference frame Σ_0. Hence, it is $l = 1, n = 0$. The dynamic model (5) reduces to the classical Euler's rotational equation of motion

$$\boldsymbol{M}\dot{\boldsymbol{\omega}} + \boldsymbol{C}(\boldsymbol{\omega})\boldsymbol{\omega} = \boldsymbol{u} \tag{34}$$

where all of the quantities are expressed in the frame Σ_1. In Eq. (34), $\boldsymbol{M}$ is the (3×3) inertia matrix, $\boldsymbol{C}(\boldsymbol{\omega}) = -\boldsymbol{S}_3(\boldsymbol{M}\boldsymbol{\omega})$, and $\boldsymbol{u}$ is the (3×1) vector of input moments from the actuators. It is assumed that the input moments can be applied continuously to the spacecraft, for example, by means of hydrazine thrusters. In practice, these thrusters can be operated in pulse mode via a closed-loop modulator scheme, which guarantees that the mean value of the modulated output follows the continuous reference input moment.[21]

Numerical simulations have been performed in the MATLAB® 5.2 with SIMULINK 2.2 environment. For the spacecraft model, the inertia matrix has been selected as

$$\boldsymbol{M} = \text{diag}\{1,\ 0.63,\ 0.85\}\ \text{kg} \cdot \text{m}^{-2}$$

the presence of white noise (with 10^{-12} power) on sensor outputs has been considered, and quantization effects have been introduced under the assumption of a 12-bit A/D converter on the attitude sensor outputs.

The case study consists of tracking a commanded trajectory constituted by a rotation of $\pi/6$ rad about the axis $[1/\sqrt{3}\ \ 1/\sqrt{3}\ \ 1/\sqrt{3}]^T$ to be performed in 2 s, according to a fifth-order polynomial time law for the desired rotation angle. At $t = 0$, the spacecraft orientation has been chosen such that the initial tracking error is $\tilde{\boldsymbol{\epsilon}}_d(0) = [-0.0044\ \ -0.0022\ \ -0.0009]^T$. Notice that the tracking error for the orientation, expressed in terms of the components of the vector part of a quaternion, is a nondimensional quantity. [See Eq. (A1).]

First, the proposed output feedback control law is adopted. In particular, Eq. (22) can be written in the form

$$\boldsymbol{u} = \boldsymbol{M}\boldsymbol{a}_r + \boldsymbol{C}(\boldsymbol{\omega}_o)\boldsymbol{\omega}_r + k_v(\boldsymbol{\omega}_r - \boldsymbol{\omega}_o) + k_p\tilde{\boldsymbol{\epsilon}}_d \tag{35}$$

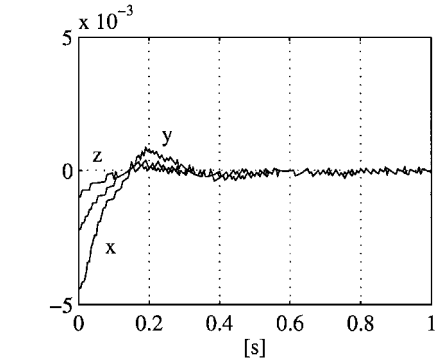

a) Tracking errors

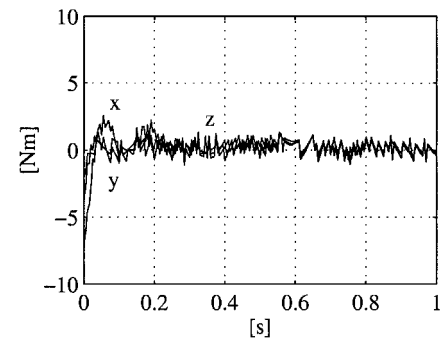

b) Control inputs

Fig. 1 Rigid spacecraft, simulation results with output feedback control law (35) and (36).

whereas the observer Eqs. (24) become

$$\dot{\boldsymbol{z}} = \boldsymbol{M}\boldsymbol{a}_r - \left(l_p + \tfrac{1}{2}l_v\lambda_e\tilde{\eta}_e\right)\tilde{\boldsymbol{\epsilon}}_e + k_p\tilde{\boldsymbol{\epsilon}}_d + \boldsymbol{C}(\boldsymbol{\omega}_o)\boldsymbol{\omega}_r + \boldsymbol{C}^T(\boldsymbol{\omega}_r)\boldsymbol{\omega}_o$$

$$\boldsymbol{\omega}_e = \boldsymbol{M}^{-1}(\boldsymbol{z} - l_v\tilde{\boldsymbol{\epsilon}}_e) - \lambda_e\tilde{\boldsymbol{\epsilon}}_e \tag{36}$$

The control gains and the observer parameters are set to $k_p = 1600$, $k_v = 35, l_p = 2400, l_v = 120$, and $\lambda_d = \lambda_e = 0.01$, whereas the inertia matrix parameters used in the control law are affected by a 40% error with respect to the values used in the model. Moreover, a numerical implementation of the control algorithm has been considered with a sampling time of 5 ms.

The results reported in Fig. 1a show that good tracking performance is obtained for the control law (35) and (36), also in the presence of model uncertainty. Notice that the control inputs are not affected by any chattering, in spite of measurement noise and quantization.

The same case study has been considered using the passivity-based control law proposed in Ref. 5, requiring full-state feedback, that is,

$$\boldsymbol{u} = \boldsymbol{M}\dot{\boldsymbol{\omega}}_r + \boldsymbol{C}(\boldsymbol{\omega})\boldsymbol{\omega}_r + k_v(\boldsymbol{\omega}_r - \boldsymbol{\omega}) + k_p\tilde{\boldsymbol{\epsilon}}_d \tag{37}$$

Because velocity measurements are not available, the angular velocity in Eq. (37) is computed by inverting the quaternion propagation rule (Appendix A), that is,

$$\boldsymbol{\omega} = 2\begin{bmatrix} -\boldsymbol{\epsilon}^T \\ \boldsymbol{E}_3(\eta, \boldsymbol{\epsilon}) \end{bmatrix}\begin{bmatrix} \dot{\eta} \\ \dot{\boldsymbol{\epsilon}} \end{bmatrix} \tag{38}$$

where $\{\eta, \boldsymbol{\epsilon}\}$ is the unit quaternion representing the actual attitude of the spacecraft (available from orientation measurements) and its time derivative is estimated by filtering $\{\eta, \boldsymbol{\epsilon}\}$ via the first-order linear system

$$s/(1 + s\tau) \tag{39}$$

with $\tau = 5$ ms. The control gains k_p and k_v in Eq. (37) have been set to the same values as those in Eq. (35).

The results reported in Fig. 2a show that tracking errors are comparable to those obtained with the output feedback control law;

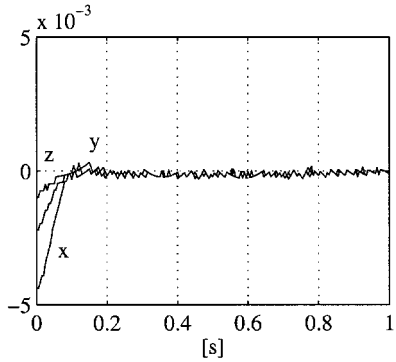

a) Tracking errors

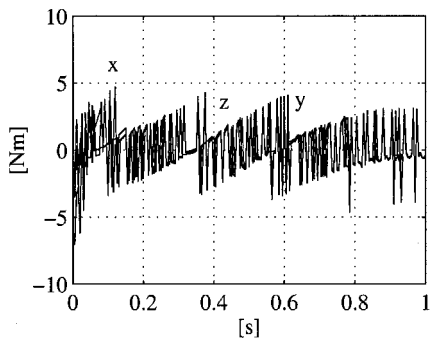

b) Control inputs

Fig. 2 Rigid spacecraft, simulation results with control law (37).

however, the control inputs (Fig. 2b) are affected by a significant chattering phenomenon. This undesirable effect could be reduced by increasing the time constant of the filter (39) at the expense of a greater tracking error.

B. Robot Manipulator

Consider a six-degree-of-freedom robot manipulator. Let $\boldsymbol{p}^0$ and $\boldsymbol{R}^0$ denote, respectively, the position vector and the rotation matrix of a frame Σ_1 attached to the end effector with respect to a base frame Σ_0. In the absence of kinematic singularities, the robot configuration can be described in terms of the set $\mathcal{X} = \{\boldsymbol{p}^0, \boldsymbol{R}^0\}$; hence, $n = 3$ and $l = 1$. The (6×1) end-effector velocity vector is given by

$$\boldsymbol{v} = \begin{bmatrix} \dot{\boldsymbol{p}}^0 \\ \boldsymbol{\omega} \end{bmatrix} \tag{40}$$

Then, the equations of the motion for the manipulator are formally identical to Eq. (5), where the vector $\boldsymbol{u}$ represents the generalized force, that is, force and moment, at the end effector. The input torques at joint actuators can be computed as

$$\boldsymbol{\tau} = \boldsymbol{J}^T(\boldsymbol{q})\boldsymbol{u} \tag{41}$$

where $\boldsymbol{q}$ is the (6×1) vector of joint variables and $\boldsymbol{J}$ is the (6×6) Jacobian matrix that is assumed to be nonsingular.

Note that the assumption of the absence of kinematic singularities is not too restrictive because an accurate motion planning for the end effector can be carried out to avoid singularities. On the other hand, when such accurate motion planning is not feasible (e.g., when the references are generated in real time), the occurrence of singularities can be handled by resorting to, for example, a damped least-squares pseudoinverse of the Jacobian (see Refs. 18 and 19).

Both a simulation and an experimental study have been carried out on an industrial robot Comau SMART-3 S. The robot manipulator has a six-revolute-joint anthropomorphic geometry, as depicted in Fig. 3, where the coordinate frames Σ_0 and Σ_1 are evidenced. The joints are actuated by brushless motors via gear trains. Shaft absolute resolvers provide motor position measurements. The robot is controlled by an open version of the C3G 9000 control unit, which has a VME-based architecture with a bus-to-bus communication

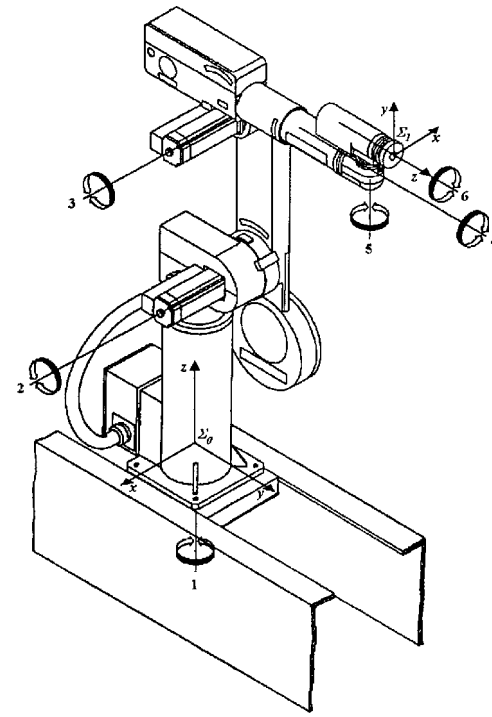

Fig. 3 Robot manipulator, geometry of six-joint manipulator.

link to a personal computer Pentium. This is in charge of computing the control algorithm and passing the references to the current servos through the communication link at a 1000-Hz sampling rate. The joint shafts are not equipped with tachometers for velocity measurements; moreover, the end-effector position and orientation are computed from joint position measurements via forward kinematics.

The dynamic model of the robot manipulator has been identified in terms of a minimum number of parameters, where the dynamics of the outer three joints have been chosen simply as purely inertial and decoupled.[22]

The case study consists of tracking a commanded trajectory for the end-effector position and orientation, starting from the rest pose. The path for the position is a straight line with a displacement $[0.2 \quad 0.2 \quad -0.8]^T$ m with respect to the base frame. At the same time, a rotation of $-\pi/2$ about the x axis of the base frame is commanded. The trajectory along the path is generated according to a fifth-order polynomial profile with null initial and final velocities and accelerations, with a 20-s duration.

First, the control law and the observer equations in Eqs. (22) and (24) are tested, with parameters $\boldsymbol{\Lambda}_d = \boldsymbol{\Lambda}_e = \text{diag}\{20\boldsymbol{I}_3, 20\boldsymbol{I}_3\}$, $\boldsymbol{K}_p = \text{diag}\{3 \cdot 10^4\boldsymbol{I}_3, 2 \cdot 10^4\boldsymbol{I}_3\}$, $\boldsymbol{K}_v = \text{diag}\{300\boldsymbol{I}_3, 50\boldsymbol{I}_3\}$, $\boldsymbol{L}_p = \text{diag}\{8 \cdot 10^3\boldsymbol{I}_3, 4 \cdot 10^3\boldsymbol{I}_3\}$, and $\boldsymbol{L}_v = \text{diag}\{600\boldsymbol{I}_3, 300\boldsymbol{I}_3\}$.

Then, the passivity-based control law,

$$\boldsymbol{u} = \boldsymbol{M}(\mathcal{X})\dot{\boldsymbol{v}}_r + \boldsymbol{C}(\mathcal{X}, \boldsymbol{v})\boldsymbol{v}_r + \boldsymbol{K}_v(\boldsymbol{v}_r - \boldsymbol{v}) + \boldsymbol{K}_p\boldsymbol{e}_d + \boldsymbol{g}(\mathcal{X}) \tag{42}$$

requiring full-state feedback is tested. The absence of velocity measurements is overcome by replacing the joint velocities by their numerical derivatives, that is, obtained via first-order difference. The gains $\boldsymbol{K}_v$ and $\boldsymbol{K}_p$ are set as they were for the output feedback controller.

1. *Simulations*

A simulation study has been worked out by considering the model of the robot manipulator just described. A discrete-time implementation of the control at a 1-ms sampling interval is assumed; also, quantization effects (16-bit A/D converter) and white noise (10^{-13} power) on the joint position measurements have been considered. Simulations have been performed in the MATLAB 5.2 with SIMULINK 2.2 environment.

The results obtained with the output feedback control law (22) and (24) are illustrated in Figs. 4 and 5. The time histories of the position and orientation errors (Fig. 4) show that good tracking is achieved,

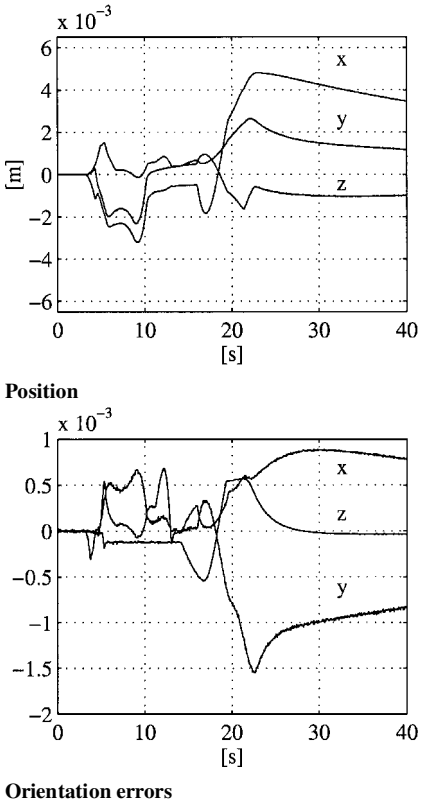

Fig. 4 Robot manipulator, simulation results with output feedback control law (22) and (24).

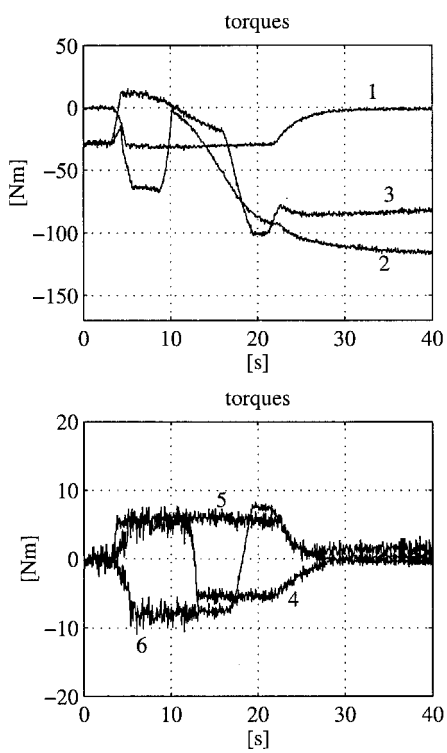

Fig. 5 Robot manipulator, simulation results with output feedback control law (22) and (24): commanded joint torques.

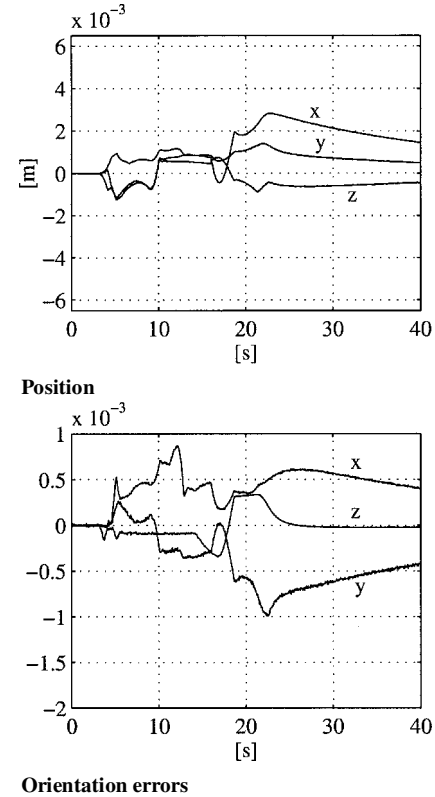

Fig. 6 Robot manipulator, simulation results with control law (42).

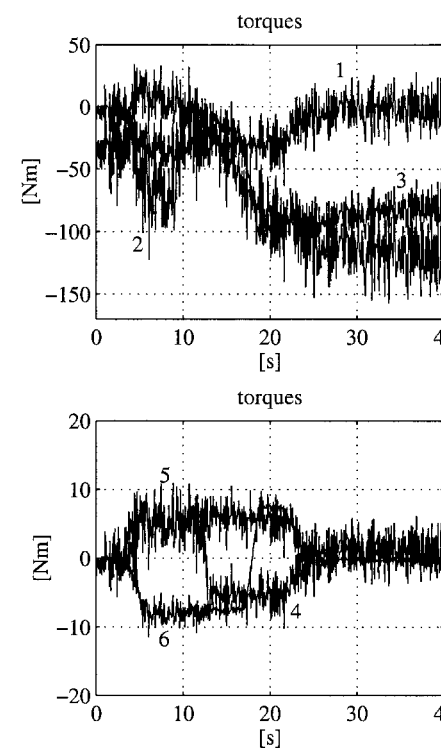

Fig. 7 Robot manipulator, simulation results with control law (42): commanded joint torques.

although a steady-state error is present due to the inaccurate compensation of friction at low velocities. Moreover, the time histories of the commanded joint torques (Fig. 5) show a small amount of noise, despite the presence of noise and quantization considered for joint position measurements.

The results obtained with the passivity-based control law (42) are reported in Figs. 6 and 7. It can be recognized that, with the chosen set of gains, the performance in terms of tracking errors is slightly better than the output feedback control law. On the other hand, the chattering of the commanded currents (Fig. 7) due to measurement noise and quantization is much greater.

2. Experiments

An experimental investigation has been carried out on the same robot to test the feasibility of the proposed approach when implemented on a conventional robotic system. It is interesting to compare the performance of the controller–observer scheme (22)

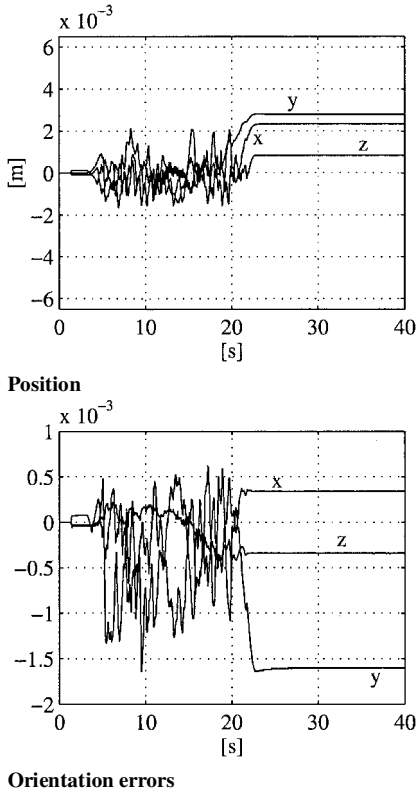

Fig. 8 Robot manipulator, experimental results with control law (22) and (24).

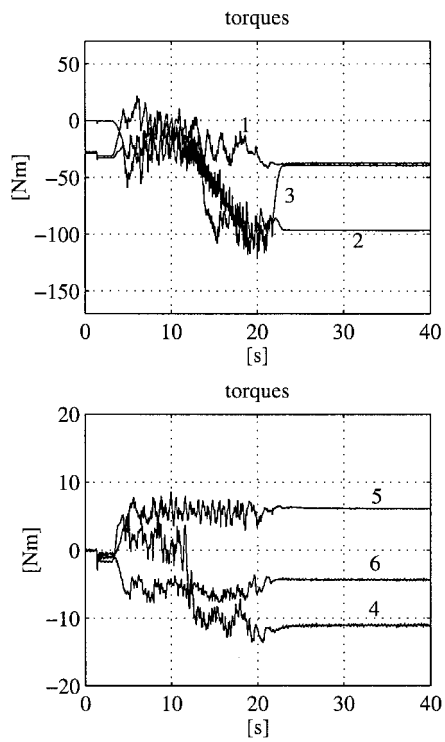

Fig. 9 Robot manipulator, experimental results with control law (22) and (24): commanded joint torques.

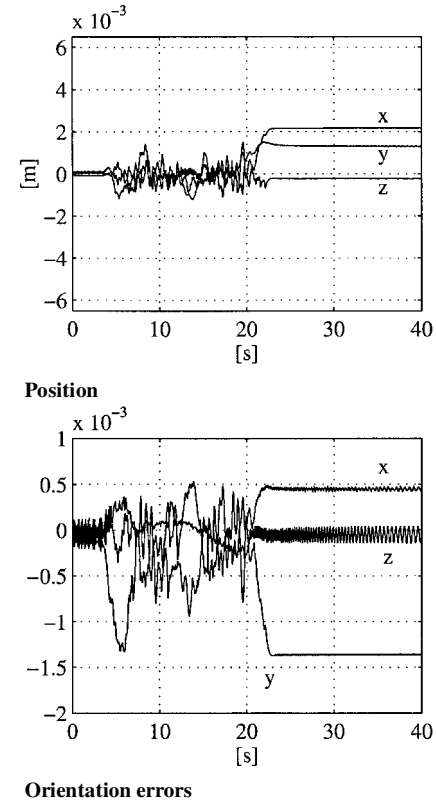

Fig. 10 Robot manipulator, experimental results with control law (42).

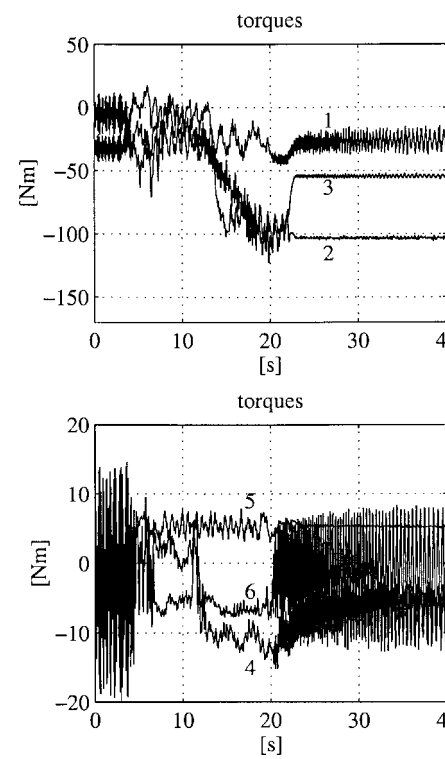

Fig. 11 Robot manipulator, experimental results with control law (42): commanded joint torques.

and (24) vs the control law (42) in detail in the presence of phenomena not modeled in the simulation, such as joint friction, backlash and elasticity of gear trains, and electromagnetic disturbances due to joint motors.

The results for the control law (22) and the observer (24) are illustrated in Figs. 8 and 9, whereas the results obtained when the control law (42) is adopted are reported in Figs. 10 and 11.

Note that the experiments confirm the simulation results. In particular, the time histories of the position and orientation errors (Figs. 8 and 10) show that good tracking is achieved for both control laws, although a steady-state error is present due to the inaccurate compensation of friction at low velocities. Note that, with the chosen set of gains, the performance in terms of tracking errors is slightly better for the control law (42). The oscillatory behavior during the motion can be ascribed to electromagnetic disturbances generated by the joint actuators; this phenomenon can be observed on the commanded joint torques as well (Figs. 9 and 11). Moreover, the presence of noisy measurements combined with nonlinear phenomena

at low velocities (friction and backlash) leads to a strong chattering on the commanded joint torques and on the orientation errors. This undesirable behavior is avoided when the proposed controller–observer scheme is adopted.

V. Conclusions

In this paper, the problem of tracking control for a class of mechanical systems has been considered. It has been assumed that the system configuration is represented by a set of generalized coordinates and by the orientation of a number of coordinate frames. A novel aspect of this problem has been investigated here, namely, the tracking of desired trajectories without using velocity measurements. A controller–observer scheme has been devised and a rigorous proof of exponential convergence of both tracking and estimation errors has been carried out by using the Lyapunov direct method. Two case studies have been developed to compare the proposed control law with a passivity-based control strategy. First, the attitude control problem of a rigid spacecraft was considered. Then, the application to position and orientation control of the end effector of a robot manipulator was performed. In the former case, only simulation results have been presented, whereas in the latter case, both simulation and experimental results have been provided that show the effectiveness of the proposed approach.

Appendix A: Unit Quaternion

The orientation of a given frame Σ_a with respect to a reference frame can be expressed via a four-parameter representation in terms of a unit quaternion, namely, Euler parameters,

$$\mathcal{Q}_a = \{\eta_a, \boldsymbol{\epsilon}_a\} = \{\cos(\theta/2), \boldsymbol{k}\sin(\theta/2)\} \tag{A1}$$

where θ and $\boldsymbol{k}$ are, respectively, the rotation and the (3×1) unit vector of an equivalent angle/axis description of orientation. Notice that the scalar part η_a and the vector part $\boldsymbol{\epsilon}_a$ of the quaternion are constrained on the unit radius sphere of $\mathbb{R}^4$, that is,

$$\eta_a^2 + \boldsymbol{\epsilon}_a^T\boldsymbol{\epsilon}_a = 1 \tag{A2}$$

Moreover, $\mathcal{Q}_a = \{\eta_a, \boldsymbol{\epsilon}_a\}$ and $\mathcal{Q}'_a = \{-\eta_a, -\boldsymbol{\epsilon}_a\}$ represent the same orientation, and frame Σ_a is aligned with the reference frame as long as $\eta_a = \pm 1$ and $\boldsymbol{\epsilon}_a = \boldsymbol{0}$.

The mutual orientation between two frames Σ_a and Σ_b can be described by the rotation matrix $\boldsymbol{R}_b^a = \boldsymbol{R}_a^T\boldsymbol{R}_b$. The corresponding unit quaternion can be either extracted directly from $\boldsymbol{R}_b^a$ (Ref. 23) or computed by composition (quaternion product) of the unit quaternions $\mathcal{Q}_a^{-1} = \{\eta_a, -\boldsymbol{\epsilon}_a\}$ and $\mathcal{Q}_b = \{\eta_b, \boldsymbol{\epsilon}_b\}$:

$$\begin{aligned}\tilde{\mathcal{Q}}_{ba} &= \left\{\tilde{\eta}_{ba}, \tilde{\boldsymbol{\epsilon}}_{ba}^a\right\} = \mathcal{Q}_a^{-1} * \mathcal{Q}_b \\ &= \left\{\eta_a\eta_b + \boldsymbol{\epsilon}_a^T\boldsymbol{\epsilon}_b, \eta_a\boldsymbol{\epsilon}_b - \eta_b\boldsymbol{\epsilon}_a - \boldsymbol{S}(\boldsymbol{\epsilon}_a)\boldsymbol{\epsilon}_b\right\}\end{aligned} \tag{A3}$$

where the asterisk denotes the quaternion product.[20] If the two frames are aligned, this product is $\boldsymbol{R}_b^a = \boldsymbol{I}_3$, where $\boldsymbol{I}_3$ denotes the (3×3) identity matrix. In this case, $\tilde{\eta}_{ba} = \pm 1$ and $\tilde{\boldsymbol{\epsilon}}_{ba}^a = \boldsymbol{0}$, and, thus, $\tilde{\boldsymbol{\epsilon}}_{ba}^a$ can be used to represent an orientation error.

The relationship between the time derivative of the quaternion components and the angular velocity $\tilde{\boldsymbol{\omega}}_{ba}^a = \boldsymbol{R}_a^T(\boldsymbol{\omega}_b - \boldsymbol{\omega}_a)$ of the frame Σ_b relative to the frame Σ_a, expressed in Σ_a, is established by the so-called quaternion propagation rule

$$\dot{\tilde{\eta}}_{ba} = -\tfrac{1}{2}\tilde{\boldsymbol{\epsilon}}_{ba}^{aT}\tilde{\boldsymbol{\omega}}_{ba}^a \tag{A4}$$

$$\dot{\tilde{\boldsymbol{\epsilon}}}_{ba}^a = \tfrac{1}{2}\boldsymbol{E}_3\left(\tilde{\eta}_{ba}, \tilde{\boldsymbol{\epsilon}}_{ba}^a\right)\tilde{\boldsymbol{\omega}}_{ba}^a \tag{A5}$$

with

$$\boldsymbol{E}_3\left(\tilde{\eta}_{ba}, \tilde{\boldsymbol{\epsilon}}_{ba}^a\right) = \tilde{\eta}_{ba}\boldsymbol{I}_3 - \boldsymbol{S}_3\left(\tilde{\boldsymbol{\epsilon}}_{ba}^a\right) \tag{A6}$$

When l different coordinate frames are considered, it is convenient to consider the set of unit quaternions $\mathcal{Q} = \{\mathcal{Q}_1, \ldots, \mathcal{Q}_l\}$ representing the orientation of the frames and the corresponding stacked vectors

$$\boldsymbol{\eta} = \begin{bmatrix}\eta_1 \\ \vdots \\ \eta_l\end{bmatrix}, \qquad \boldsymbol{\epsilon} = \begin{bmatrix}\boldsymbol{\epsilon}_1 \\ \vdots \\ \boldsymbol{\epsilon}_l\end{bmatrix} \tag{A7}$$

Hence, the representation of l mutual orientations can be expressed in terms of the stacked vectors $\tilde{\boldsymbol{\eta}}$ and $\tilde{\boldsymbol{\epsilon}}$. Moreover, when the stacked velocity vector $\tilde{\boldsymbol{\omega}}$ and the diagonal matrices are defined,

$$\boldsymbol{N}(\tilde{\boldsymbol{\epsilon}}) = \operatorname{diag}\left\{\tilde{\boldsymbol{\epsilon}}_1^T, \ldots, \tilde{\boldsymbol{\epsilon}}_l^T\right\}$$

$$\boldsymbol{E}(\tilde{\boldsymbol{\eta}}, \tilde{\boldsymbol{\epsilon}}) = \operatorname{diag}\{\boldsymbol{E}_3(\tilde{\eta}_1, \tilde{\boldsymbol{\epsilon}}_1), \ldots, \boldsymbol{E}_3(\tilde{\eta}_l, \tilde{\boldsymbol{\epsilon}}_l)\}$$

the propagation rule can be generalized as follows:

$$\dot{\tilde{\boldsymbol{\eta}}} = -\tfrac{1}{2}\boldsymbol{N}(\tilde{\boldsymbol{\epsilon}})\tilde{\boldsymbol{\omega}} \tag{A8}$$

$$\dot{\tilde{\boldsymbol{\epsilon}}} = \tfrac{1}{2}\boldsymbol{E}(\tilde{\boldsymbol{\eta}}, \tilde{\boldsymbol{\epsilon}})\tilde{\boldsymbol{\omega}} \tag{A9}$$

Appendix B: Proof of Theorem 1

Consider the positive-definite Lyapunov function candidate

$$\begin{aligned}V = {} & \frac{1}{2}\boldsymbol{\sigma}_d^T\boldsymbol{M}(\mathcal{X})\boldsymbol{\sigma}_d + \frac{1}{2}\boldsymbol{\sigma}_e^T\boldsymbol{M}(\mathcal{X})\boldsymbol{\sigma}_e \\ & + \frac{1}{2}\tilde{\boldsymbol{x}}_d^T\boldsymbol{K}_{pX}\tilde{\boldsymbol{x}}_d + \sum_{i=1}^{l} k_{pOi}\left[(1-\tilde{\eta}_{di})^2 + \tilde{\boldsymbol{\epsilon}}_{di}^T\tilde{\boldsymbol{\epsilon}}_{di}\right] \\ & + \frac{1}{2}\tilde{\boldsymbol{x}}_e^T\boldsymbol{L}_{pX}\tilde{\boldsymbol{x}}_e + \sum_{i=1}^{l} l_{pOi}\left[(1-\tilde{\eta}_{ei})^2 + \tilde{\boldsymbol{\epsilon}}_{ei}^T\tilde{\boldsymbol{\epsilon}}_{ei}\right]\end{aligned} \tag{B1}$$

In view of property 3 and of the propagation rule (A4) and (A5), the time derivative of V along the trajectories of the closed-loop system (31) and (32) is given by

$$\begin{aligned}\dot{V} = {} & -\boldsymbol{\sigma}_d^T\boldsymbol{K}_v\boldsymbol{\sigma}_d - \boldsymbol{e}_{de}^T\boldsymbol{\Lambda}_d\boldsymbol{K}_p\boldsymbol{e}_d - \boldsymbol{e}_e^T\boldsymbol{\Lambda}_e\boldsymbol{L}_p\boldsymbol{e}_e \\ & - \boldsymbol{\sigma}_e^T[\boldsymbol{L}_v\boldsymbol{A}(\tilde{\boldsymbol{\eta}}_e, \tilde{\boldsymbol{\epsilon}}_e) - \boldsymbol{K}_v]\boldsymbol{\sigma}_e - \boldsymbol{\sigma}_d^T\boldsymbol{C}(\mathcal{X}, \boldsymbol{\sigma}_e)\boldsymbol{v}_r \\ & + \boldsymbol{\sigma}_e^T\boldsymbol{C}^T(\mathcal{X}, \boldsymbol{\sigma}_d)\boldsymbol{v}_o - \boldsymbol{\sigma}_d^T\boldsymbol{M}(\mathcal{X})\boldsymbol{S}_O(\tilde{\boldsymbol{\omega}}_d)\boldsymbol{v}_d\end{aligned} \tag{B2}$$

In the following, it is assumed that $\tilde{\eta}_{di} > 0$ and $\tilde{\eta}_{ei} > 0$ $(i = 1, \ldots, l)$. When the angle/axis interpretation of the unit quaternion is considered, the preceding assumption corresponds to considering orientation errors characterized by angular displacements in the range $]-\pi, \pi[$.

Note that the equality, where $i = 1, \ldots, l$,

$$\tilde{\boldsymbol{\epsilon}}_{dei}^T\tilde{\boldsymbol{\epsilon}}_{di} = \tilde{\eta}_{ei}\tilde{\boldsymbol{\epsilon}}_{di}^T\tilde{\boldsymbol{\epsilon}}_{di} - \tilde{\eta}_{di}\tilde{\boldsymbol{\epsilon}}_{di}^T\tilde{\boldsymbol{\epsilon}}_{ei}$$

implies that

$$\begin{aligned}\boldsymbol{e}_{de}^T\boldsymbol{\Lambda}_d\boldsymbol{K}_p\boldsymbol{e}_d = {} & \tilde{\boldsymbol{x}}_d^T\boldsymbol{\Lambda}_{dX}\boldsymbol{K}_{pX}\tilde{\boldsymbol{x}}_d - \tilde{\boldsymbol{x}}_d^T\boldsymbol{\Lambda}_{dX}\boldsymbol{K}_{pX}\tilde{\boldsymbol{x}}_e \\ & + \sum_{i=1}^{l}\lambda_{dOi}k_{pOi}\tilde{\eta}_{ei}\|\tilde{\boldsymbol{\epsilon}}_{di}\|^2 - \sum_{i=1}^{l}\lambda_{dOi}k_{pOi}\tilde{\eta}_{di}\tilde{\boldsymbol{\epsilon}}_{di}^T\tilde{\boldsymbol{\epsilon}}_{ei}\end{aligned}$$

and, thus,

$$\boldsymbol{e}_{de}^T\boldsymbol{\Lambda}_d\boldsymbol{K}_p\boldsymbol{e}_d \geq k_{pm}\tilde{\eta}_{em}\|\boldsymbol{e}_d\|^2 - k_{pM}\|\boldsymbol{e}_d\|\|\boldsymbol{e}_e\| \tag{B3}$$

where k_{pm} (k_{pM}) is the minimum (maximum) eigenvalue of the matrix $\boldsymbol{\Lambda}_d\boldsymbol{K}_p$, and $\tilde{\eta}_{em} = \min_i\{\tilde{\eta}_{ei}\}$. Moreover, in view of the block diagonal structure of the matrix $\boldsymbol{L}_v$ and of the skew symmetry of the matrix $\boldsymbol{S}_3(\cdot)$, the following inequality holds:

$$\boldsymbol{\sigma}_e^T\boldsymbol{L}_v\boldsymbol{A}(\tilde{\boldsymbol{\eta}}_e, \tilde{\boldsymbol{\epsilon}}_e)\boldsymbol{\sigma}_e \geq \tfrac{1}{2}l_{vm}\tilde{\eta}_{em}\|\boldsymbol{\sigma}_e\|^2 \tag{B4}$$

where l_{vm} is the minimum eigenvalue of the matrix $\boldsymbol{\Lambda}_v$.

In view of properties 1 and 3 and Eqs. (20), (29), (B3), and (B4), and when it is taken into account that $\boldsymbol{v} = \boldsymbol{v}_d - \tilde{\boldsymbol{v}}_d$ with $\|\boldsymbol{v}_d\| \leq v_{dM}$, the function $\dot{V}$ can be upper bounded as

$$\dot{V} \le -k_{vm}\|\boldsymbol{\sigma}_d\|^2 - k_{pm}\tilde{\eta}_{em}\|\boldsymbol{e}_d\|^2 - (l_{vm}/2)\tilde{\eta}_{em}\|\boldsymbol{\sigma}_e\|^2 + k_{vM}\|\boldsymbol{\sigma}_e\|^2 - l_{pm}\|\boldsymbol{e}_e\|^2 + k_{pM}\|\boldsymbol{e}_d\|\|\boldsymbol{e}_e\| + C_M\|\boldsymbol{\sigma}_d\|\|\boldsymbol{\sigma}_e\|(2\|\tilde{\boldsymbol{\nu}}_d\| + 2v_{dM} + \|\boldsymbol{\sigma}_d\| + \|\boldsymbol{\sigma}_e\|) + M_M v_{dM}\|\boldsymbol{\sigma}_d\|\|\tilde{\boldsymbol{\nu}}_d\| \tag{B5}$$

where k_{vm} (k_{vM}) denotes the minimum (maximum) eigenvalue of the matrix $\boldsymbol{K}_v$ and l_{pm} is the minimum eigenvalue of the matrix $\boldsymbol{\Lambda}_e\boldsymbol{L}_p$.

Consider the state-space domain defined as follows

$$B_\rho = \{\boldsymbol{\zeta} : \|\boldsymbol{\zeta}\| < \rho,\ \rho < 1\} \tag{B6}$$

with $\tilde{\eta}_{di} > 0$ and $\tilde{\eta}_{ei} > 0$ ($i = 1, \ldots, m$). In B_ρ, the following inequality holds

$$\|\tilde{\boldsymbol{\nu}}_d\| = \|\boldsymbol{\sigma}_d - \boldsymbol{\Lambda}_d\boldsymbol{e}_{de}\| \le (1 + 2\lambda_{dM})\rho \tag{B7}$$

where λ_{dM} denotes the maximum eigenvalue of the matrix $\boldsymbol{\Lambda}_d$ and the inequality

$$\|\boldsymbol{e}_{de}\| \le \|\boldsymbol{e}_d\| + \|\boldsymbol{e}_e\| \tag{B8}$$

has been used, which can be derived from Eqs. (18) and (19) when Eqs. (A2) and (A3) are taken into account.

When the squares in Eq. (B5) are completed, and by the use of inequality (B7), it follows that

$$\dot{V} \le -(k_{vm} - \beta(1 + \lambda_{dM}) - C_M(\alpha + \rho))\|\boldsymbol{\sigma}_d\|^2 - \left(\frac{l_{vm}}{2}\tilde{\eta}_{em} - k_{vM} - C_M(\alpha + \rho)\right)\|\boldsymbol{\sigma}_e\|^2 - \frac{1}{2}(k_{pm}\tilde{\eta}_{em} - \lambda_{dM}\beta)\|\boldsymbol{e}_d\|^2 - \frac{1}{2}(l_{pm} - \lambda_{dM}\beta)\|\boldsymbol{e}_e\|^2 - \frac{1}{2}\begin{bmatrix}\|\boldsymbol{e}_d\|\\ \|\boldsymbol{e}_e\|\end{bmatrix}^T\begin{bmatrix}k_{pm}\tilde{\eta}_{em} & -k_{pM}\\ -k_{pM} & l_{pm}\end{bmatrix}\begin{bmatrix}\|\boldsymbol{e}_d\|\\ \|\boldsymbol{e}_e\|\end{bmatrix} \tag{B9}$$

where $\alpha = (1 + 2\lambda_{dM})\rho + v_{dM}$ and $\beta = M_M v_{dM}$. Hence, there exists a scalar $\kappa > 0$ such that

$$\dot{V} \le -\kappa\|\boldsymbol{\zeta}\|^2 \tag{B10}$$

in the domain B_ρ, provided that the controller and observer parameters satisfy the inequalities

$$k_{pm} > \beta\lambda_{dM}\Big/\sqrt{1 - \rho^2} \tag{B11}$$

$$k_{vm} > C_M(\alpha + \rho) + \beta(1 + \lambda_{dM}) \tag{B12}$$

$$l_{pm} > \max\left\{k_{pM}^2\Big/k_{pm}\sqrt{1 - \rho^2},\ \beta\lambda_{dM}\right\} \tag{B13}$$

$$l_{vm} > \left(2\Big/\sqrt{1 - \rho^2}\right)[k_{vM} + C_M(\alpha + \rho)] \tag{B14}$$

where the inequality $0 < \tilde{\eta}_{em} < \sqrt{(1 - \rho^2)} < 1$ has been exploited.

Therefore, given a domain B_ρ, characterized by any $\rho < 1$, there always exists a set of observer and controller gains such that $\dot{V} \le 0$ in B_ρ. Moreover, for $\tilde{\eta}_{di} \ge 0$ and $\tilde{\eta}_{ei} \ge 0$ ($i = 1, \ldots, l$), the following inequality holds:

$$0 \le (1 - \tilde{\eta}_{di})^2 \le (1 - \tilde{\eta}_{di})(1 + \tilde{\eta}_{di}) = \|\tilde{\boldsymbol{\epsilon}}_{di}\|^2$$

and a similar inequality can be written in terms of $\tilde{\eta}_{ei}$ and $\tilde{\boldsymbol{\epsilon}}_{ei}$. Hence, function V can be bounded as

$$c_m\|\boldsymbol{\zeta}\|^2 \le V(\boldsymbol{\zeta}) \le c_M\|\boldsymbol{\zeta}\|^2 \tag{B15}$$

with

$$c_m = \tfrac{1}{2}\min\left\{M_m, k'_{pm}, l'_{pm}\right\}, \qquad c_M = \tfrac{1}{2}\max\left\{M_M, 4k'_{pM}, 4l'_{pM}\right\}$$

where k'_{pm} (k'_{pM}) is the minimum (maximum) eigenvalue of the matrix $\boldsymbol{K}_p$ and l'_{pm} (l'_{pM}) is the minimum (maximum) eigenvalue of the matrix $\boldsymbol{L}_p$.

Because $V(t)$ is a decreasing function along the system trajectories, the inequality (B15) guarantees that, for a given $0 < \rho < 1$, all of the trajectories $\boldsymbol{\zeta}(t)$ starting in the domain

$$\Omega_\rho = \left\{\boldsymbol{\zeta} : \|\boldsymbol{\zeta}\| < \rho\sqrt{c_m/c_M}\right\} \tag{B16}$$

remain in the domain B_ρ for all $t > 0$, provided that $\tilde{\eta}_{di}(t) > 0$ and $\tilde{\eta}_{ei}(t) > 0$, $i = 1, \ldots, l$, for all $t > 0$. The latter condition is fulfilled when $\tilde{\eta}_{di}(0)$ and $\tilde{\eta}_{ei}(0)$ are positive. In fact, $\|\tilde{\boldsymbol{\epsilon}}_{di}\| < \rho < 1$ and $\|\tilde{\boldsymbol{\epsilon}}_{ei}\| < \rho < 1$ for all $t > 0$ implies that $\tilde{\eta}_{di}(t)$ and $\tilde{\eta}_{ei}(t)$ cannot change their signs.

Moreover, from inequalities (B10) and (B15), the convergence in the domain B_ρ is exponential,[24] which implies exponential convergence of $\boldsymbol{e}_d$, $\boldsymbol{e}_e$, $\tilde{\boldsymbol{\nu}}_d$, and $\tilde{\boldsymbol{\nu}}_e$.

The condition $\rho < 1$ is due to the unit norm constraint on the quaternion components and gives a rather conservative estimate of the domain of attraction. Note, however, that this limitation arises when spheres are used to estimate the domain of attraction. Better estimates can be obtained by the use of the domains of different shapes, for example, ellipsoids.

Acknowledgments

This work was supported in part by Ministero dell'Università e della Ricerca Scientifica e Tecnologica and by Agenzia Spaziale Italiana.

References

[1]Lian, K.-Y., Wang, L.-S., and Fu, L.-C., "Globally Valid Adaptive Controllers of Mechanical Systems," *IEEE Transactions on Automatic Control*, Vol. 42, 1997, pp. 1149–1154.

[2]Roberson, R. E., and Schwertassek, R., *Dynamics of Multibody Systems*, Springer-Verlag, Berlin, 1988.

[3]Wie, B., Weiss, H., and Araposthatis, A., "Quaternion Feedback Regulator for Spacecraft Eigenaxis Rotations," *Journal of Guidance, Control, and Dynamics*, Vol. 12, 1989, pp. 375–380.

[4]Wen, J. T., and Kreutz-Delgado, K., "The Attitude Control Problem," *IEEE Transactions on Automatic Control*, Vol. 36, 1991, pp. 1148–1162.

[5]Egeland, O., and Godhavn, J. M., "Passivity-Based Adaptive Attitude Control of a Rigid Spacecraft," *IEEE Transactions on Automatic Control*, Vol. 39, 1994, pp. 842–846.

[6]Salcudean, S. E., "A Globally Convergent Angular Velocity Observer for Rigid Body Motion," *IEEE Transactions on Automatic Control*, Vol. 36, 1991, pp. 1493–1497.

[7]Lizarralde, F., and Wen, J. T., "Attitude Control Without Angular Velocity Measurement: A Passivity Approach," *IEEE Transactions on Automatic Control*, Vol. 41, 1996, pp. 468–472.

[8]Costic, B. T., Dawson, D. M., de Queiroz, M. S., and Kapila, V., "Quaternion-Based Adaptive Attitude Tracking Controller Without Velocity Measurements," *Journal of Guidance, Control, and Dynamics*, Vol. 24, 2001, pp. 1214–1222.

[9]Nicosia, S., and Tomei, P., "Robot Control by Using Only Position Measurements," *IEEE Transactions on Automatic Control*, Vol. 35, 1990, pp. 1058–1061.

[10]Berghuis, H., and Nijmeijer, H., "A Passivity Approach to Controller–Observer Design for Robots," *IEEE Transactions on Robotics and Automation*, Vol. 9, 1993, pp. 740–754.

[11]Berghuis, H., and Nijmeijer, H., "Global Regulation of Robots Using Only Position Measurements," *Systems and Control Letters*, Vol. 21, 1993, pp. 289–293.

[12]Caccavale, F., Natale, C., and Villani, L., "Task-Space Tracking Control Without Velocity Measurements," *1999 IEEE Conference on Robotics and Automation*, IEEE Publications, Piscataway, NJ, 1999, pp. 512–517.

[13]Canudas de Wit, C., and Fixot, N., "Adaptive Control of Robot Manipulators via Velocity Estimated Feedback," *IEEE Transactions on Automatic Control*, Vol. 37, 1992, pp. 1234–1237.

[14]Kim, Y. H., and Lewis, F. L., "Neural Network Output Feedback Control of Robot Manipulators," *IEEE Transactions on Robotics and Automation*, Vol. 15, 1999, pp. 301–309.

[15]Caccavale, F., and Villani, L., "Output Feedback Control for Attitude Tracking," *Systems and Control Letters*, Vol. 38, 1999, pp. 91–98.

[16]Ortega, R., Lorìa, A., Nicklasson, P., and Sira-Ramìrez, H., *Passivity-Based Control of Euler–Lagrange Systems: Mechanical, Electrical and Electromechanical Applications*, Springer-Verlag, London, 1998.

[17]Sciavicco, L., and Siciliano, B., *Modelling and Control of Robot Manipulators*, 2nd ed., Springer-Verlag, London, 2000.

[18]Caccavale, F., Chiaverini, S., and Siciliano, B., "Second-Order Kinematic Control of Robot Manipulators with Jacobian Damped Least-Squares Inverse: Theory and Experiments," *IEEE/ASME Transactions on Mechatronics*, Vol. 2, 1997, pp. 188–194.

[19]Kircanski, M., Kircanski, N., Lekovic, D., and Vukobratovic, M., "An Experimental Study of Resolved Acceleration Control at Singularities: Damped Least-Squares Approach," *Journal of Dynamic Systems, Measurement and Control*, Vol. 119, 1997, pp. 97–101.

[20]Chou, J. C. K., "Quaternion Kinematic and Dynamic Differential Equations," *IEEE Transactions on Robotics and Automation*, Vol. 1, 1992, pp. 53–64.

[21]Cavallo, A., De Maria, G., and Ferrara, F., "Attitude Control for Low Lift/Drag Reentry Vehicles," *Journal of Guidance, Control, and Dynamics*, Vol. 19, 1996, pp. 816–822.

[22]Antonelli, G., Caccavale, F., and Chiacchio, P., "A Systematic Procedure for the Identification of Dynamic Parameters of Robot Manipulators," *Robotica*, Vol. 17, 1999, pp. 427–435.

[23]Shepperd, S. W., "Quaternion from Rotation Matrix," *Journal of Guidance and Control*, Vol. 1, 1978, pp. 223, 224.

[24]Khalil, H. K., *Nonlinear Systems*, 2nd ed., Prentice–Hall, Upper Saddle River, NJ, 1996.